LBNL-48606

Liquid-Film Assisted Formation of Alumina/Niobium Interfaces

Joshua D. Sugar, Joseph T. McKeown, Robert A. Marks & Andreas M. Glaeser*

Department of Materials Science and Engineering,
University of California,
&
Center for Advanced Materials
Lawrence Berkeley National Laboratory, Berkeley, CA 94720

Abstract

Alumina has been joined at 1400°C using niobium-based interlayers. Two different joining approaches were compared: solid-state diffusion bonding using a niobium foil as an interlayer, and liquid-film assisted bonding using a multilayer copper/niobium/copper interlayer. In both cases, a 127-μm thick niobium foil was used; ≈1.4-μm or ≈3-μm thick copper films flanked the niobium. Room-temperature four-point bend tests showed that the introduction of a copper film had a significant beneficial effect on the average strength and the strength distribution. Experiments using sapphire substrates indicated that during bonding the initially continuous copper film evolved into isolated copper-rich droplets/particles at the sapphire/interlayer interface, and extensive regions of direct bonding between sapphire and niobium. Film breakup appeared to initiate at either niobium grain boundary ridges, or at asperities or irregularities on the niobium surface that caused localized contact with the sapphire.

Keywords: ceramic/metal interfaces, joining, diffusion bonding, brazing, transient liquid phase bonding, transient liquid phase, alumina, sapphire, niobium, copper, dewetting, grain boundary grooving, fracture

*Fellow, American Ceramic Society

Introduction

The processing of ceramic-metal interfaces, which are a critical feature in many materials systems, is fundamental to successful fabrication of a wide range of assemblies and devices. Solid-state methods (diffusion bonding) and methods that exploit a liquid phase (brazing and soldering) are among the techniques that have been most widely studied as a means of generating high-performance joints involving ceramics (ceramic/ceramic or ceramic/metal joints) [1-5]. Over the last decade, an increasing level of effort has been devoted to developing joining techniques that exploit a transient liquid phase (TLP) to join ceramics [6-26] as well as metals [*e.g.*, [27] and references therein].

Diffusion bonding and brazing each have unique advantages, but also liabilities that increase in number and severity as the processing temperature is increased. Solid-state diffusion bonding allows the use of refractory interlayers and thereby has the potential to produce joints that will exhibit high strength at elevated temperature. Joining proceeds under an applied pressure and at an elevated temperature designed to allow adequate mass transport for ceramic/metal interface formation and concurrent interfacial void elimination. Reactive metal brazing imposes somewhat less stringent demands on surface flatness, does not require a substantial bonding pressure, and is more conducive to mass production. Although more refractory brazes can, in principle, be developed, the most widely used braze formulations offer limited temperature capability, and joints remelt at relatively low temperature.

Joining methods that exploit a transient liquid phase have the potential to incorporate some of the more attractive features of both diffusion bonding and brazing while avoiding many of their limitations. The development of a liquid phase at the joining temperature leverages some of the surface preparation and bonding pressure advantages of brazing. More modest joining temperatures help to mitigate the microstructural degradation and chemical reaction that become increasingly problematic at higher joining temperatures. Isothermal disappearance of the liquid and the development of a refractory interlayer preserve the possibility of high-temperature service.

Prior work using multilayer copper/niobium/copper interlayers to join alumina [19] demonstrated that strong joints could be produced at 1150°C, well below the temperatures normally used for solid-state

diffusion bonding of niobium to alumina. The present work is part of a broader effort [26, 52, 53] to examine the effects of processing conditions on joint properties and to establish fundamental processing-microstructure-property relationships for this system. This paper provides the first direct comparison of the strength and fracture behavior of alumina/niobium interfaces (joints) prepared at the same temperature (1400°C) and applied pressure (≈2.2 MPa) by conventional solid-state diffusion bonding and by liquid-phase-assisted diffusion bonding. Fractographs and studies of interface microstructure evolution in sapphire/copper/niobium bonds indicate that the liquid copper film accelerates contact formation and ultimately dewets the interface, yielding comparatively more extensive alumina/niobium contact and improved strength characteristics. Fractography results also suggest that the local alumina microstructure influences the crack path for near-interfacial failures.

Background

Alumina/niobium and sapphire/niobium have served as model ceramic/metal systems for nearly three decades. The diffusion bonding of these materials, their interfacial structure, chemical compatibility, strength and failure characteristics, and the influence of interfacial impurities have all been examined and reported extensively in the literature [28-51]. Extensive discussions can be found in prior publications [19, 26, 52, 53]. For the present purposes, a brief review of diffusion bonding conditions, interface microstructure evolution, and fracture properties is provided. Salient findings of prior work using multilayer copper/niobium/copper interlayers are also summarized.

Alumina/Niobium Diffusion Bonding

The range of time-temperature-bonding load conditions used in diffusion bonding sapphire or alumina to niobium is broad. Generally, for conventional high-vacuum (HV; ≈10^{-3} Pa) diffusion bonding, bonding temperatures were 1500-1950°C, bonding times were typically several hours, and the applied load was generally of the order of 10 MPa [28, 32, 36, 37, 54]. The use of ultrahigh-vacuum (UHV; ≈10^{-8} Pa) conditions coupled with sputter cleaning of the bonding surfaces [38] has been shown to reduce the bonding temperatures by up to 500°C relative to HV bonding. However, in both HV and UHV bonds,

fracture energies increased with bonding temperature, a trend attributed to a concurrent increase in the area fraction bonded. "Typical" UHV bonding conditions for niobium/sapphire involved 3 h at 1400°C with an applied load of 10 MPa, and allowed the fabrication of well-bonded couples with high fracture energies.

Mechanical tests of joints in which oriented sapphire and oriented niobium single crystals were bonded have shown that the fracture energy G_c is very sensitive to the interface crystallography, with values ranging from ≈60 [44] to ≈2400 J/m^2 [55] in room-temperature tests. Joints between polycrystalline niobium and polycrystalline alumina typically exhibited either lower fracture energies [34] or fracture energies nearer to the lower bicrystal values [55]. A limited number of strength measurements indicated that joints processed at 1600°C under HV conditions failed at tensile stresses of the order of 100-150 MPa [28, 32].

Reimanis [45] and Gibbesch and Elssner [46] have examined the evolution of the pore structure at the ceramic/metal interface. Gibbesch and Elssner bonded polycrystalline alumina using 2-mm thick, 99.99% pure niobium plates under UHV conditions; the applied pressure was 10 MPa and temperature was varied from 900°C to 1500°C. The area fraction bonded increased with increasing bonding temperature. Plastic deformation of the metal was deemed the dominant mechanism of pore closure at the interface. In contrast, Reimanis [45] bonded sapphire single crystals of two different orientations to (111)-textured 100-200-μm thick, 99.9% pure niobium foils at 1450°C under an applied pressure of 2 MPa. Removal of interfacial porosity as a result of further annealing at 1450°C was monitored by optical microscopy. The study indicated that: 1) pore removal proceeded by the growth of highly facetted bonding fronts whose facet structure was related to the orientation of niobium grains, 2) pore removal rates in samples annealed with and without a 2 MPa pressure were similar, and 3) grain boundary grooves in the niobium foil appeared to provide the initial contact points with the sapphire, and played a key role in the development of new bonded regions. Notably, significant unbonded regions persisted even after 18 h at 1450°C.[⋆]

[⋆] Morozumi *et al.* [32] reported ≈50% bonded area after 1 h, 8.8 MPa, HV bonding at 1600°C. Turwitt *et al.* [34] reported that after a 2 h, 10 MPa, HV bonding cycle at 1700°C, ≈10-20% of the interface remained unbonded, suggesting that porosity removal is slow even at substantially higher temperature. However, Gibbesch and Elssner [46] reported ≈98% bonded area after 1 h, 10 MPa, UHV bonding at 1600°C.

Bonding with Copper/Niobium/Copper Interlayers

Several studies have been performed in which multilayer copper/niobium/copper interlayers were used to bond a specific 99.5% pure polycrystalline alumina. Bonding temperature and bonding pressure were varied. A comparison of work by Shalz *et al.* [19] (1150°C, 5.1 MPa) and that of Marks [26, 52, 53] (1150°C, 2.2 MPa and 7.5 MPa) suggests that increasing the pressure at 1150°C led to higher average fracture strength and reduced scatter. The improved strength characteristics appeared to correlate with more complete breakup of the copper film, which was initially ≈3 μm thick in all three cases. For samples bonded at 1150°C, most bend beams failed along the alumina/interlayer interface. Experiments by Marks *et al.* [26, 52, 53] demonstrated that increasing the processing temperature to 1400°C while maintaining a bonding pressure of ≈2.2 MPa produced samples with high average room-temperature bend strength (240 MPa), a narrow strength distribution (standard deviation ±18 MPa), and a roughly 3:1 ratio of ceramic to interfacial failures.

Characterization of the interfacial microstructure in sapphire couples processed at 1400°C for 6 h showed a relatively wide variation in the extent of dewetting of the liquid copper film [26]. Comparisons of different regions suggested that contact between the sapphire and the niobium initiated along the niobium grain boundary groove ridges that formed due to "etching" by the copper-rich liquid film. In bonds with polycrystalline alumina, the degree of film breakup appeared to be higher, suggesting that alumina grain boundaries and cavities may help initiate breakup [26]. Comparison of fracture surfaces from interfacial failures in bonds prepared at 1400°C from a relatively coarser (≈20-25 μm) and a finer (≈1 μm) average grain size alumina also suggested that the alumina grain boundaries and the grain boundary periodicity influenced the film evolution and fracture surface topography [53].

Experimental Procedure

Many of the materials and experimental procedures used in this work duplicate those used previously, and further details are available elsewhere [19, 26]. Briefly, the bonding surface of 19.5 mm × 19.5 mm × 22.5 mm blocks of a 99.5% pure alumina (Coors Technical Ceramics Co., Oak Ridge, TN) were polished using successively finer diamond suspensions. After polishing with 1 μm grit size suspension,

a final polish was performed with colloidal silica. Joints were also fabricated using ≈0.5-mm thick, high-purity, optical finish, sapphire substrates (Meller Optics Inc., Providence, RI) that required no additional polishing; the c-axes of the substrates were within ±≈1° of the surface normal.

As in prior studies, a flattened and cleaned 99.99% pure, 127-μm thick niobium foil (Goodfellow, Berwyn, PA), and a commercial copper wire (Consolidated Companies Wire and Associated, Chicago, IL) served as the materials used to form the interlayers. Copper films ≈1.4 μm or ≈3 μm thick were deposited directly onto the cleaned and polished alumina or sapphire surfaces by evaporation of the copper source in a high vacuum chamber. Film thickness was determined using both profilometry (Tencor Instruments Inc., San Jose, CA) and weight gain measurements as described previously [19].

Polycrystalline alumina assemblies were bonded for 6 h at 1400°C in a graphite element vacuum hot press using an applied load of ≈2.2 MPa. Sapphire assemblies were bonded and given post-bonding anneals at 1150°C; the bonding duration and load were 6 h and ≈1.8 MPa.† Heating and cooling rates to and from the bonding temperature were typically 4°C/min and 2°C/min, respectively. After bonding, the polycrystalline alumina assemblies were cut into beams ≈3 mm × ≈3 mm in cross section and 4-5 cm in length, with the metal interlayer at the beam center. The tensile surface of each beam was polished to a 1-μm finish and edges were bevelled to remove machining flaws that could initiate failure. Beams were tested at room temperature using four-point bending. The inner and outer spans were 9 and 25 mm, respectively. Testing was done with a displacement rate of 0.05 mm/min. Strengths were calculated from the load at failure using standard relationships derived for monolithic elastic materials. Two independent assessments [17, 53] have shown that under identical testing conditions, the average four-point bend strength of (unbonded) alumina beams prepared from the same source material is ≈280 MPa.

Relevant surfaces and interfaces were characterized at various stages of processing and property measurement. The surface roughness of both the as-ground and polished alumina blocks, as well as the roughness of the niobium foil before and after flattening, were assessed by profilometry to permit a

† In a prior study [26], sapphire samples bonded for 6 h at 1400°C showed a wide variation in interfacial microstructure and generally a high degree of film breakup. In an effort to retard the kinetics, and to better assess the evolution process, the bonding and annealing temperatures for the present experiments were reduced to 1150°C.

comparison of the surface roughness of the substrates and interlayer and the copper film thickness. Results are summarized in TABLE I, and discussed further in subsequent sections. For bonds made using sapphire, the sapphire/interlayer microstructure evolution was monitored using optical microscopy. Fiducial marks were introduced on the external sapphire surface so that fixed positions could be located easily. Samples were examined both in the as-processed state and after prolonged periods of post-bonding anneal; microstructure-time sequences were constructed. For failures in which fracture proceeded primarily along or near one alumina/interlayer interface, fracture surfaces were examined. All diffusion-bonded samples (no copper) exhibited interfacial/near-interfacial failures. For bonds prepared with copper, up to 75% of the fractures were purely ceramic failures. For selected samples in which failure progressed along or near the alumina/interlayer interface, beam fracture surfaces were mounted adjacent to one another so that equivalent fractographic locations were in mirror symmetry positions. The general microstructure at matching locations, the pore structure, and the fracture path could thus be readily identified. Fracture surfaces were first inspected using optical microscopy, and then examined using scanning electron microscopy (SEM) (ISI DS130) and energy dispersive spectroscopy (EDS).

Results and Discussion

Room-Temperature Mechanical Properties

The beneficial effect of thin liquid copper films on the strength characteristics of bonded assemblies is illustrated in FIGURE 1. Solid-state diffusion bonding at 1400°C using a relatively modest bonding pressure (2.2 MPa) led to relatively low average bend strengths (103 MPa ± 20 MPa), and a Weibull modulus of only ≈5.5. All failures in the tested samples proceeded primarily along the alumina/niobium interface, with significant tearing of the niobium. As will be shown subsequently, for the diffusion-bonded samples, large areas in which the alumina and niobium fail to achieve contact remain. The combination of a relatively higher degree of interfacial porosity coupled with large isolated unbonded regions promoted interfacial failure at low applied stress. A plate cut from the diffusion-bonded block was given further vacuum annealing for 12 h at 1400°C without any applied pressure. This plate failed during

the cutting associated with beam preparation, and thus, no substantial strengthening (contact growth) appears to have occurred, presumably due to the low rate of solid-state diffusion.

The inclusion of as little as a 1.4-μm thick copper film allows for void filling by liquid flow, and provides a conduit for rapid transport of niobium. As shown in TABLE I, the average roughness of the polished alumina (30 nm) and of the flattened niobium foil (275 nm) are less than the copper film thickness. It is thus reasonable to assume that the amount of liquid formed will be sufficient to fill many interfacial gaps, and thus reduce the area fraction and severity of unbonded regions along the alumina/interlayer interface.[✣] At 1400°C, copper dissolves ≈3 at % niobium [56]. When coupled with a diffusion coefficient for niobium in liquid copper that is expected to be orders of magnitude higher than the self-diffusion coefficient for niobium, a considerable enhancement in the rate of niobium redistribution can be expected relative to that in solid-state diffusion bonding. The filling of interfacial voids by the liquid, transport of niobium through the liquid to shrink or eliminate larger interfacial flaws (gaps), and dewetting of the liquid film ultimately lead to a higher area fraction of alumina-niobium contact and a decrease in the number and severity of interfacial flaws. Although failures continued to proceed primarily along the alumina/interlayer interface, with more limited departures into the niobium, the average fracture stress increased to 197 MPa (±37 MPa). The weakest beam prepared with 1.4 μm thick copper had a fracture strength (136 MPa) comparable to that of the strongest diffusion-bonded specimen (155 MPa). The Weibull modulus, ≈5.6, is essentially the same as that for diffusion bonding (5.5).

A further improvement in the fracture behavior occurs as the liquid film thickness is increased from 1.4 μm to 3 μm. Although the increase in mean strength is more modest, from 197 MPa to 240 MPa, the standard deviation diminishes by roughly a factor of two (from 37 to 18 MPa) and ≈75% of the samples tested are characterized by failures that initiate within the ceramic and generally propagate entirely within the ceramic. As shown in FIGURE 1, interfacial failures do not necessarily occur at lower stresses; the average fracture strengths and standard deviations for ceramic (243 MPa ± 18 MPa) and interfacial failures (236

[✣] The profilometry results suggest that the use of as-ground substrates may have little detrimental effect on the strength since the roughness is still less than the liquid film thickness. It is, however, likely that the worst flaws and the largest unbonded regions reflect longer wavelength variations and larger departures from planarity than indicated by the profilometry results.

MPa ± 19 MPa) are essentially indistinguishable. The Weibull modulus increases to ≈15, and is comparable to that of the unbonded reference alumina (≈14). Prior work [53] utilizing the same processing temperature and comparable film thickness has shown that the use of a higher strength ceramic further improves the strength characteristics. It is uncertain whether additional improvements would be realized by employing even thicker copper films. Prior work has suggested that reduced strengths result when the area fraction of copper along the alumina/interlayer interface increases [53]. Ongoing studies are addressing this issue.

Fractography and Chemical Analysis

Fractography was performed on diffusion-bonded samples and samples prepared with a copper film. The focus was on regions of the fracture surface near the tensile surface of the beams. Representative areas are shown in Figures 2-4. When both metal and ceramic sides of the fracture surface are shown, the tensile edge lies near the abutting edges of the micrographs.

Fractography of a diffusion-bonded sample with a failure stress of 79 MPa is shown in Figure 2. Figures 2*a* and 2*b* provide matching regions of the metal side and the ceramic side of the fracture surface, respectively. Three major types of regions can be distinguished. Large featureless regions such as those labeled ***a*** in Figure 2*a* correspond to regions in which the ceramic grain boundaries (see corresponding region in Figure 2*b*) have not been imprinted on the metal, indicating a lack of contact. The area fraction of such unbonded regions on the fracture surface appears to decrease as the fracture strength increases. Careful examination of fracture surfaces shows regions in which the growth fronts of alumina-niobium contact zones are facetted, as originally described by Reimanis [45]. An enlargement of such a growth front, evident in Figure 2*a*, is provided as Figure 2*c*. Roughness striations, labeled ***b*** in Figure 2*b*, are found at matching locations on both the ceramic and metal sides of the fracture surface. These striations appear to reflect the irregularities in the surface finish of the niobium foil; the asperity ridges in the foil will first contact the alumina and influence the local alumina surface topography. Such regions also appear to diminish as the fracture strength increases. There are relatively few interfacial fracture regions in which the metal foil shows a well-defined imprint of the ceramic grain boundaries, suggesting that the dissolution of

alumina and the grooving of boundaries is limited. As the strength increases, a somewhat more complete mapping of the ceramic microstructure onto the interlayer is indicated. Finally, there are regions in which the fracture surface takes on a mottled or dimpled appearance, and a darker contrast in the images. An SEM image of the ceramic side of such a region, FIGURE 2*d*, and the EDS map of this same region, FIGURE 2*e*, indicate that niobium has been torn and has adhered to the ceramic. A small peak due to silicon is also found in these regions, signaling that the small amount of glassy phase present in the material may play a role in bonding, as discussed by De Graef *et al.* [57] for platinum/alumina interfaces. The alumina used has a bimodal grain size distribution. It is noteworthy that the interfacial failure occurs primarily in regions with the coarser grain size, and that tearing of the niobium correlates well with the finer grain size regions in the alumina. Such a correlation was not noted in our prior studies [19, 26, 53].

The introduction of copper has a noticeable effect on the strength distribution. When the fracture surfaces of diffusion-bonded samples and those with 1.4 μm copper are compared, some similarities and some differences are apparent. FIGURES 3*a* and 3*b* show the metal and ceramic sides of a sample with 1.4 μm copper and a fracture strength of 197 MPa. As in diffusion-bonded samples, the failures are primarily interfacial, and localized tearing of the niobium is seen, indicating that the crack front undergoes localized excursions into the interlayer, but is then drawn back to the interface. Tearing of the niobium again correlates with the finer grain size regions in the alumina. In general, although some regions of incomplete contact persist (again marked ***a***), there appears to be a more complete "printing" of the ceramic microstructure onto the metal foil, and the roughness striations are absent. These changes presumably reflect the effect of the liquid metal on grain boundary grooving kinetics [58, 59] and foil surface smoothing kinetics, as well as niobium dissolution to saturate the copper liquid film. For a 1.4-μm film thickness, the breakup of the copper film (discussed in detail in the subsequent section) appears to be complete, and relatively few discrete copper particles are seen on the fracture surfaces. However, when present, they do appear on both sides of the fracture surface (see locations marked ①, ②, and ③), indicating that the ductile metal tears during fracture.

Increasing the copper film thickness to 3 μm leads to a preponderance of ceramic failures. Of the samples that failed along the interface, the metal and ceramic fracture surfaces of the sample exhibiting the

lowest strength (206 MPa) are shown in Figures 4*a* and 4*b*, respectively. As expected, more copper particles are evident than in the 1.4 μm copper film samples; these particles tear during fracture, as exemplified by the copper particle labeled ① on both surfaces. Although there is more copper liquid present, regions remain in which contact between the interlayer and the ceramic is lacking. An example is marked ***a*** in Figure 4*a*, and many more similar regions are present (in this particularly weak sample). The region labeled ***b*** in Figure 4*b* represents a cavity in the alumina surface due to pullout of an alumina grain. The grain is evident on the metal side, Figure 4*a*, at the matching location. When viewed in color, it is clear that copper is present underneath this pulled-out grain. Similar observations were reported previously by Shalz *et al.* [19].

The area fractions of interfacial failure were determined for several samples within each of the sample sets examined using a point counting method. Increasing the copper thickness affected not only the strength, but also the fracture path. In comparing the fracture surfaces of samples prepared with 0-μm, 1.4-μm, and 3.0-μm thick copper films, the average area fraction of interfacial failure was ≈48(±5)%, ≈67(±6)%, and ≈96(±3)%, respectively. In samples with no copper and with 1.4 μm copper films, tearing of the interlayer occurred.

For all samples, micrographs of matching areas of both sides of the fractured sample were taken. By comparing the degree to which the ceramic microstructure was imprinted on the metal surface, it was easiest to identify those regions in which contact was not achieved during bonding (see, *e.g.*, regions ***a*** in Figures 2*a-b*). Adherent islands of metal (or silicide) on the ceramic surface obscured up to ≈½ of the alumina/interlayer interface area in some samples. The observable regions of contact are thus only within the fraction of the total fracture surface associated with interfacial failure. Assuming that regions in which the crack deviates from the alumina/interlayer interface are associated with complete ceramic/interlayer contact gives an upper limit on the area fraction of contact. Alternatively, if the interfacial porosity is more uniformly distributed, then the average area fraction of contact would be given by the area fraction of contact within the regions of interfacial failure. Both values show an increase in contact with increasing copper film thickness. The latter interpretation seems to better rationalize the significant strength

differences between diffusion-bonded and liquid-phase bonded samples. Both values are provided in Table II.✦

interfacial microstructure evolution

The absence or presence of a copper film and the breakup of an initially continuous copper film into isolated copper droplets along the interlayer/alumina interface clearly have an effect on the joint properties. In prior work [26, 53], bonds prepared at 1400°C using sapphire single crystals rather than polycrystalline alumina provided some information on the nature of the interface microstructure that develops during bonding, and provided some insight on the evolution mechanism. Although the microstructure varied with interface position, the observations suggested that initial contact between the niobium and sapphire occurred along niobium grain boundary ridges, thereby isolating patches of liquid copper atop individual niobium grains. The edges of these thin liquid patches then underwent a morphological instability similar to that observed during high-temperature crack healing. The liquid phase thus serves a dual function. In the short term, it allows for void filling along the interface. It also provides a high-diffusivity path for niobium transport, and liquid-phase-assisted growth of contact area between the sapphire and niobium during liquid film breakup.

In the sapphire-based bonds prepared at 1150°C as part of this study, a much more limited degree of film breakup was evident following bonding. This is likely due to the combined effect of a lower diffusivity of niobium in liquid copper and lower solubility of niobium in copper at 1150°C relative to 1400°C. Thus, samples bonded at 1150°C provided an opportunity to examine the evolution of the interfacial microstructure.

Figure 5 shows a series of optical micrographs taken at two different locations along the interface of a sapphire-based joint prepared at 1150°C. Figures 5*a* and 5*c* show the interfacial microstructures after a 6 h bonding cycle, and a 9 h post-bonding anneal at 1150°C with no applied load. There is very little indication of interfacial porosity, however, the area fraction of niobium/sapphire contact is low in both

✦ We note that ≈75% of the samples prepared with 3-μm thick copper films failed in the ceramic. It is possible that the few samples that failed at the interface are not representative of the average, and that the level of interfacial porosity is higher than that of a typical interface in this group of samples.

cases. The samples were given additional 7 h anneals, and the interfacial microstructures were examined after each anneal. Micrographs illustrating the regions in Figures 5*a* and 5*c* after a total of 29 h at 1150°C are shown in Figures 5*b* and 5*d*, respectively. In the Figure 5*a*-5*b* sequence, *lines* of niobium/sapphire contact develop and persist. It appears that grain boundaries in the niobium play the major role in initiating film breakup, and copper remains trapped in the grain boundary groove, thereby outlining the niobium grains. These observations are thus somewhat reminiscent of those reported by Reimanis for solid-state diffusion bonding, however, the liquid enhances the rate of contact formation, and facetted fronts do not develop. In the Figure 5*c*-5*d* sequence, *points* of contact develop with time, suggesting that irregularities in the surfaces, most likely asperities in the niobium foil surface, can also provide sites of contact initiation. These differences in evolution patterns may reflect statistical differences in the nature of the niobium foil. More generally, surface roughness may increase the number of contact points and accelerate the growth of sapphire/niobium contact area. (Grain boundaries and other periodic irregularities in the surface of polycrystalline alumina substrates contribute to the higher degree of film breakup after bonding than is observed with sapphire.) Experiments in which the surface finish of the alumina is varied are in progress. Lithographic patterning of sapphire surfaces may also provide a means of assessing the effect of surface roughness. It is clear that in both cases, the area fraction of sapphire/niobium contact increases with time. The rate of sapphire/niobium contact area increase would be expected to increase with increasing load, decreasing yield strength of niobium, and increasing niobium solubility-diffusivity product, *i.e.*, increasing temperature.

The polycrystalline nature of the niobium foil and variations in the foil thickness and local roughness are believed to contribute to the substantial spatial variability in the microstructure. The grain boundary misorientation varies from grain to grain, causing a spatial variation in the grain boundary groove angle and grooving kinetics. Small variations in the foil thickness stemming from rolling can induce significant variations in the liquid film thickness and the ridge height that must be achieved to initiate sapphire/niobium contact. Optical micrographs of the flattened foils show variations in the surface roughness. It is not entirely surprising that substantial variations in the microstructure are evident. When polycrystalline alumina substrates are used instead of sapphire, defects in the ceramic surface, grain-to-grain

variations in the alumina surface orientation, and alumina grain boundary groove characteristics can all be important, and appear to accelerate film breakup and reduce the spatial scale of variability in microstructural evolution.

Summary and Conclusions

A comparison of the fracture characteristics of polycrystalline alumina assemblies joined using niobium interlayers and copper/niobium/copper interlayers at 1400°C indicates that the copper has a strong beneficial effect. Strength increases and the standard deviation decreases as the copper film thickness is increased. The initially continuous liquid film provides a high transport rate path for dissolved niobium, and can flow to fill interfacial voids. The area fraction of contact between the alumina and the interlayer appears to be increased when copper is present. Fracture paths are affected by the introduction of copper as well, with progressively less tearing of the niobium interlayer and a transition to ceramic failure as the copper thickness is increased to 3 μm.

Fractography of polycrystalline alumina-based joints shows that rather than persisting as a continuous layer of copper, the film evolves into a set of discrete copper particles that lie along the alumina/interlayer interface. Model experiments using sapphire indicate that dewetting of the copper film initiates where grain boundary groove ridges in the niobium or asperities in the niobium form lines or points of contact with the alumina. The dewetting results in a high area fraction of alumina/niobium contact along the interface. Independent studies [26, 53] have shown that as a result of this interfacial microstructure, useful levels of strength can be maintained to temperatures as high as 1200°C, *i.e.*, above the melting point of copper.

Such observations suggest that the use of multilayer interlayers in which thin liquid-forming layers undergo similar morphological changes may provide a new strategy for producing joints that are useful at elevated temperatures. Since the phase diagram and kinetic considerations in selecting such liquid formers differ from those for more traditional implementations of PTLP bonding, this may provide additional options for interlayer design.

Acknowledgements

This research was supported by the Director, Office of Science, Office of Basic Energy Sciences, Division of Materials Sciences and Engineering, of the U.S. Department of Energy under Contract No. DE-AC03-76SF00098.

References

1. M. G. Nicholas and D. A. Mortimer, "Ceramic/metal joining for structural applications," *Mater. Sci. Tech.*, **1**, [9], 657-65 (1985).
2. K. Suganuma, Y. Miyamoto, and M. Koizumi, "Joining of Ceramics and Metals," *Ann. Rev. Mater. Sci.*, **18**, 33-47 (1988).
3. R. E. Loehman and A. P. Tomsia, "Joining of ceramics," *Am. Ceram. Soc. Bull.*, **67**, [2], 375-80 (1988).
4. G. Elssner and G. Petzow, "Metal/Ceramic Joining," *ISIJ Int.*, **30**, [12], 1011-1032 (1990).
5. M. G. Nicholas, Joining of ceramics, 1st ed. London ; New York: Published on behalf of the Institute of Ceramics by Chapman and Hall, 1990.
6. R. E. Loehman, "Transient Liquid Phase Bonding of Silicon Nitride Ceramics," in Surfaces and interfaces in ceramic and ceramic-metal systems, J. A. Pask and A. G. Evans, Eds. New York: Plenum Press, 1981, pp. 701-711.
7. R. D. Brittain, S. M. Johnson, R. H. Lamoreaux, and D. J. Rowcliffe, "High-temperature chemical phenomena affecting silicon nitride joints," *J. Am. Ceram. Soc.*, **67**, [8], 522-6 (1984).
8. M. L. Mecartney, R. Sinclair, and R. E. Loehman, "Silicon nitride joining," *J. Am. Ceram. Soc.*, **68**, [9], 472-8 (1985).
9. S. M. Johnson and D. J. Rowcliffe, "Mechanical properties of joined silicon nitride," *J. Am. Ceram. Soc.*, **68**, [9], 468-72 (1985).
10. S. Baik and R. Raj, "Liquid-phase bonding of silicon nitride ceramics," *J. Am. Ceram. Soc.*, **70**, [5], C105-7 (1987).
11. P. A. Walls and M. Ueki, "Mechanical properties of β-SiAlON ceramics joined using composite β-SiAlON-glass adhesives," *J. Am. Ceram. Soc.*, **78**, [4], 999-1005 (1995).
12. M. Gopal, L. C. De Jonghe, and G. Thomas, "Silicon nitride: from sintering to joining," *Acta Mater.*, **46**, [7], 2401-5 (1998).
13. S. J. Glass, F. M. Mahoney, B. Quillan, J. P. Pollinger, and R. E. Loehman, "Refractory oxynitride joints in silicon nitride," *Acta Mater.*, **46**, [7], 2393-9 (1998).
14. T. Iseki, K. Yamashita, and H. Suzuki, "Joining of self-bonded SiC by Ge metal," *Proc. Brit. Ceram. Soc.*, **31**, 1-8 (1981).
15. T. Iseki, K. Yamashita, and H. Suzuki, "Joining of self-bonded silicon carbide by germanium metal," *J. Am. Ceram. Soc.*, **64**, [1], C13-14 (1981).
16. Y. Iino, "Partial transient liquid-phase metals layer technique of ceramic-metal bonding," *J. Mater. Sci. Lett.*, **10**, [2], 104-6 (1991).
17. M. L. Shalz, B. J. Dalgleish, A. P. Tomsia, and A. M. Glaeser, "Ceramic joining. I. Partial transient liquid-phase bonding of alumina *via* Cu/Pt interlayers," *J. Mater. Sci.*, **28**, [6], 1673-84 (1993).
18. M. L. Shalz, B. J. Dalgleish, A. P. Tomsia, and A. M. Glaeser, "Ceramic joining II. Partial transient liquid-phase bonding of alumina *via* Cu/Ni/Cu multilayer interlayers," *J. Mater. Sci.*, **29**, [12], 3200-8 (1994).
19. M. L. Shalz, B. J. Dalgleish, A. P. Tomsia, R. M. Cannon, and A. M. Glaeser, "Ceramic joining III. Bonding of alumina *via* Cu/Nb/Cu interlayers," *J. Mater. Sci.*, **29**, [14], 3678-90 (1994).
20. B. J. Dalgleish, A. P. Tomsia, K. Nakashima, M. R. Locatelli, and A. M. Glaeser, "Low temperature routes to joining ceramics for high-temperature applications," *Scripta Metall. Mater.*, **31**, [8], 1043-8 (1994).

21. M. R. Locatelli, A. P. Tomsia, K. Nakashima, B. J. Dalgleish, and A. M. Glaeser, "New strategies for joining ceramics for high-temperature applications," *Key Eng. Mater.*, **111-112**, 157-90 (1995).
22. B. J. Dalgleish, K. Nakashima, M. R. Locatelli, A. P. Tomsia, and A. M. Glaeser, "New Approaches to Joining Ceramics for High-Temperature Applications," *Ceram. Int.*, **23**, [4], 313-22 (1997).
23. G. Ceccone, M. G. Nicholas, S. D. Peteves, A. P. Tomsia, B. J. Dalgleish, and A. M. Glaeser, "An evaluation of the partial transient liquid phase bonding of Si_3N_4 using Au coated Ni-22Cr foils," *Acta Mater.*, **44**, [2], 657-67 (1996).
24. M. Paulasto, G. Ceccone, and S. D. Peteves, "Joining of silicon nitride via a transient liquid," *Scripta Mater.*, **36**, [10], 1167-73 (1997).
25. S. D. Peteves, M. Paulasto, G. Ceccone, and V. Stamos, "The reactive route to ceramic joining: fabrication, interfacial chemistry and joint properties," *Acta Mater.*, **46**, [7], 2407-14 (1998).
26. R. A. Marks, D. R. Chapman, D. T. Danielson, and A. M. Glaeser, "Joining of alumina via copper/niobium/copper interlayers," *Acta Mater.*, **48**, [18-19], 4425-38 (2000).
27. W. F. Gale and Y. Guan, "Microstructure and mechanical properties of transient liquid phase bonds between NiAl and a nickel-base superalloy," *J. Mater. Sci.*, **34**, [5], 1061-71 (1999).
28. G. Elssner and G. Petzow, "Verträglichkeit zwischen Materialkomponentent in Metall-Keramik-Verbundwerkstoffen," *Z. Metallkde.*, **64**, [4], 280-86 (1973).
29. G. Elssner and R. Pabst, "Bruchmechanische Untersuchung der Haftung bei Metall-Keramik-Verbundwerkstoffen," *High Temp.-High Press.*, **6**, 321-327 (1974).
30. G. Elssner, S. Riedel, and R. Pabst, "Fractography and Fracture Paths in Ceramic-Metal Composites," *Prakt. Metall.*, **12**, 234-43 (1975).
31. G. Elssner, H. Jehn, and E. Fromm, "Influence of gas impurities on the solid-state bonding of Nb/Al_2O_3 composites above 1200°C," *High Temp.-High Press.*, **10**, [5], 487-92 (1978).
32. S. Morozumi, M. Kikuchi, and T. Nishino, "Bonding mechanism between alumina and niobium," *J. Mater. Sci.*, **16**, [8], 2137-44 (1981).
33. M. Florjancic, W. Mader, M. Ruhle, and M. Turwitt, "HREM and diffraction studies of an Al_2O_3/Nb interface," *J. de Physique*, **46**, [Supplement C4], 129-33 (1985).
34. M. Turwitt, G. Elssner, and G. Petzow, "Manufacturing and mechanical properties of interfaces between sapphire and niobium," *J. de Physique*, **46**, [Supplement C4], 123-7 (1985).
35. M. Backhaus-Ricoult, "Diffusion processes and interphase boundary morphology in ternary metal-ceramic systems," *Ber. Bunsenges. Phys. Chem.*, **90**, [8], 684-90 (1986).
36. M. Rühle, K. Burger, and W. Mader, "Structure and chemistry of grain boundaries in ceramics and of metal/ceramic interfaces," *J. Microsc. Spectrosc. Electron. (France)*, **11**, 163-77 (1986).
37. K. Burger, W. Mader, and M. Rühle, "Structure, chemistry and diffusion bonding of metal/ceramic interfaces," *Ultramicroscopy*, **22**, 1-13 (1987).
38. H. F. Fischmeister, W. Mader, B. Gibbesch, and G. Elssner, "Preparation, Properties, and Structure of Metal/Oxide Interfaces," in Interfacial structure, properties, and design, vol. 122, *Mat. Res. Soc. Proc.*, W. A. T. Clark, C. L. Briant, and M. H. Yoo, Eds. Pittsburgh, Pa.: Materials Research Society, 1988, pp. 529-540.
39. W. Mader and M. Rühle, "Electron microscopy studies of defects at diffusion-bonded Nb/Al_2O_3 interfaces," *Acta Metall.*, **37**, [3], 853-66 (1989).
40. M. Kuwabara, J. C. H. Spence, and M. Ruhle, "On the atomic structure of the Nb/Al_2O_3 interface and the growth of Al_2O_3 particles," *J. Mater. Res.*, **4**, [4], 972-7 (1989).

41. K. Burger and M. Rühle, "Material transport mechanisms during the diffusion bonding of niobium to Al_2O_3," *Ultramicroscopy*, **29**, [1-4], 88-97 (1989).
42. F. S. Ohuchi, "Surface science studies of Nb-(0001)Al_2O_3 interfacial reactions (in diffusion bonding)," *J. Mater. Sci. Lett.*, **8**, [12], 1427-9 (1989).
43. J. Mayer, C. P. Flynn, and M. Ruhle, "High-resolution electron microscopy studies of Nb/Al_2O_3 interfaces," *Ultramicroscopy*, **33**, [1], 51-61 (1990).
44. D. Korn, G. Elssner, H. F. Fischmeister, and M. Rühle, "Influence of interface impurities on the fracture energy of UHV bonded niobium-sapphire bicrystals," *Acta Metall. Mater.*, **40**, [Supplement], S355-60 (1992).
45. I. E. Reimanis, "Pore removal during diffusion bonding of Nb-Al_2O_3 interfaces," *Acta Metall. Mater.*, **40**, [Supplement], S67-74 (1992).
46. B. Gibbesch and G. Elssner, "Ultra high vacuum diffusion bonded Nb-Al_2O_3 and Cu-Al_2O_3 joints-the role of welding temperature and sputter cleaning," *Acta Metall. Mater.*, **40**, [Supplement], S59-66 (1992).
47. G. Elssner, D. Korn, and M. Rühle, "The influence of interface impurities on fracture energy of UHV diffusion bonded metal-ceramic bicrystals," *Scripta Metall. Mater.*, **31**, [8], 1037-42 (1994).
48. V. Gupta, J. Wu, and A. N. Pronin, "Effect of substrate orientation, roughness, and film deposition mode on the tensile strength and toughness of niobium-sapphire interfaces," *J. Am. Ceram. Soc.*, **80**, [12], 3172-80 (1997).
49. G. Soyez, G. Elssner, M. Ruhle, and R. Raj, "Constrained yielding in niobium single crystals bonded to sapphire," *Acta Mater.*, **46**, [10], 3571-81 (1998).
50. I. G. Batirev, A. Alavi, M. W. Finnis, and T. Deutsch, "First-principles calculations of the ideal cleavage energy of bulk niobium(111)/α-alumina(0001) interfaces," *Phys. Rev. Lett.*, **82**, [7], 1510-13 (1999).
51. W. Zhang and J. R. Smith, "Stoichiometry and adhesion of Nb/Al_2O_3," *Phys. Rev. B*, **61**, [24], 16883-9 (2000).
52. R. A. Marks, "Joining of Alumina and Sapphire via Multilayer Cu/Nb/Cu Interlayers," M.S. Thesis, Department of Materials Science and Mineral Engineering, University of California, Berkeley, (2000).
53. R. A. Marks, J. D. Sugar, and A. M. Glaeser, "Ceramic Joining IV. Effects of Processing Conditions on the Properties of Alumina Joined *via* Cu/Nb/Cu Interlayers," *J. Mater. Sci.*, **36**, [23], 5609-5624 (2001).
54. M. Rühle, M. Backhaus-Ricoult, K. Burger, and W. Mader, "Diffusion Bonding of Metal/Ceramic Interfaces – A Model Study at the Nb/Al_2O_3 Interfaces," in Ceramic Microstructures '86, J. A. Pask and A. G. Evans, Eds. New York: Plenum Press, 1987, pp. 295-305.
55. B. Gibbesch, G. Elssner, W. Mader, and H. F. Fischmeister, "Ultrahigh Vacuum Diffusion Bonding of Nb and Cu Single Crystals to Sapphire," in Joining ceramics, glass, and metal, W. Kraft and Deutsche Gesellschaft für Metallkunde, Eds. Oberursel: DGM Informationsgesellschaft, 1989, pp. 65-72.
56. T. B. Massalski, H. Okamoto, and ASM International, Binary alloy phase diagrams, 2nd ed. Materials Park, Ohio: ASM International, 1990.
57. M. De Graef, B. J. Dalgleish, M. R. Turner, and A. G. Evans, "Interfaces between alumina and platinum: structure, bonding and fracture resistance," *Acta Metall. Mater.*, **40**, [Supplement], S333-44 (1992).

58. E. Saiz, A. P. Tomsia, and R. M. Cannon, "Wetting and Work of Adhesion in Oxide/Metal Systems," in Ceramic Microstructures: Control at the Atomic Level, A. P. Tomsia and A. M. Glaeser, Eds. New York: Plenum Press, 1998, pp. 65-82.
59. E. Saiz, R. M. Cannon, and A. P. Tomsia, "Energetics and atomic transport at liquid metal/Al_2O_3 interfaces," *Acta Mater.*, **47**, [15], 4209-20 (1999).

Tables

Table I: Average surface roughness*

Material	Average Roughness
Unpolished alumina	275 nm
Polished alumina	30 nm
As-received niobium	100 nm
"Flattened" niobium	275 nm

* The initial contact of the profilometer defines zero elevation. During a scan across the substrate, the absolute values of the elevation relative to this reference are recorded at a number of points, and then averaged to provide the average roughness.

Table II: fracture path and contact area statistics

	Fracture path Statistics		Area Fraction Bonded	
	Area Fraction Interfacial Failure	Area Fraction Interlayer or Ceramic Failure	$1-\frac{Area_{unbonded}}{Area_{fracture\ surface}}$	$1-\frac{Area_{unbonded}}{Area_{interfacial\ failure}}$
Diffusion bond				
79 MPa	0.495	0.505	0.812	0.621
102 MPa	0.473	0.527	0.809	0.572
119 MPa	0.54	0.46	0.813	0.595
1.4 μm copper				
136 MPa	0.695	0.305	0.84	0.77
197 MPa	0.665	0.335	0.877	0.808
260 MPa	0.68	0.32	0.938	0.908
			0.	
3.0 μm copper				
206 MPa	0.965	0.035	0.843	0.837

Figure Captions:

Figure 1 Plot of failure probability versus beam fracture strength illustrating the beneficial effect of a thin copper film on joint characteristics. All 28 diffusion-bonded beams and all 24 of the beams prepared with 1.4-μm copper films failed along the alumina/interlayer interface. Interfacial failures are indicated by filled symbols. Of the 42 beams prepared with 3.0-μm thick copper films, 30 failed within the ceramic. Ceramic failures are indicated by open symbols. The alumina reference material was unbonded and not annealed prior to testing.

Figure 2 Optical micrographs of matching regions of *a*) metal and *b*) ceramic sides of fracture surfaces of a diffusion-bonded sample that failed at 79 MPa. Regions of facetted contact growth in the upper right hand section of Figure 2*a* are shown at higher magnification in (*c*). Figures 2*d* and 2*e* show an SEM micrograph and an EDS map of the same location on the ceramic side of the fracture surface, respectively; the roughened regions on the fracture surface correspond to niobium (blue in the EDS map) adhering to the alumina (gold in the EDS map).

Figure 3 Optical micrographs of matching regions of the *a*) metal and *b*) ceramic sides of fracture surfaces of a sample with 1.4-μm copper films assisting diffusion bonding. A more complete mapping of the ceramic grain structure onto the metal foil is evident. Matching regions of incomplete bonding are labeled ***a*** on both images; note the triple junction in the alumina is absent on the metal side due to an interfacial void that prevents contact. Most copper particles ruptured during fracture, and copper is thus present on both sides of the fracture surface; some pairs are labeled ①, ②, and ③.

Figure 4 Optical micrographs of matching regions of the *a*) metal and *b*) ceramic sides of fracture surfaces of a sample prepared with 3-μm thick copper films. Regions of incomplete bonding remain evident, one of which is labeled ***a*** in Figure 4*a*. The region marked ***b*** in Figure 4*b* represents an alumina grain that has been pulled out, and that has adhered to the metal side. Most copper particles ruptured during fracture and are present on both sides of the fracture surface; one pair is labeled ①.

Figure 5 Illustration of interfacial microstructures in two sapphire/copper/niobium couples bonded at 1150°C. Figures 5*a* and 5*b* show the interfacial microstructure after 15 h at 1150°C, and after an additional 14 h of annealing at 1150°C, respectively. In this region, grain boundary groove ridges play a major role in initiating dewetting. In Figures 5*c* and 5*d*, also showing interfacial microstructures immediately after 15 h and 29 h at 1150°C, asperities appear to play a more prominent role in initiating dewetting.

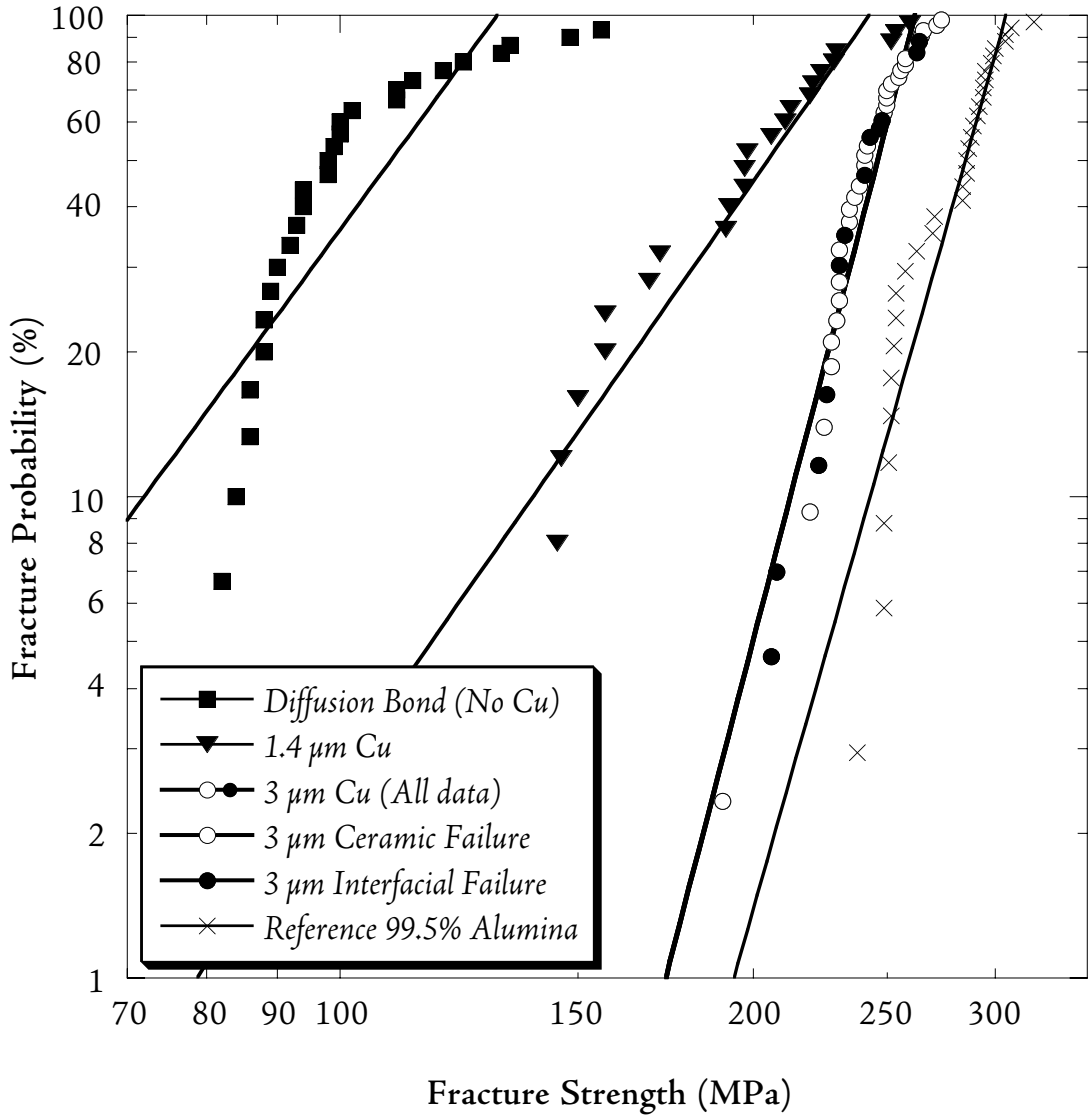

FIGURE 1 Plot of failure probability versus beam fracture strength illustrating the beneficial effect of a thin copper film on joint characteristics. All 28 diffusion-bonded beams and all 24 of the beams prepared with 1.4-μm copper films failed along the alumina/interlayer interface. Interfacial failures are indicated by filled symbols. Of the 42 beams prepared with 3.0-μm thick copper films, 30 failed within the ceramic. Ceramic failures are indicated by open symbols. The alumina reference material was unbonded and not annealed prior to testing.

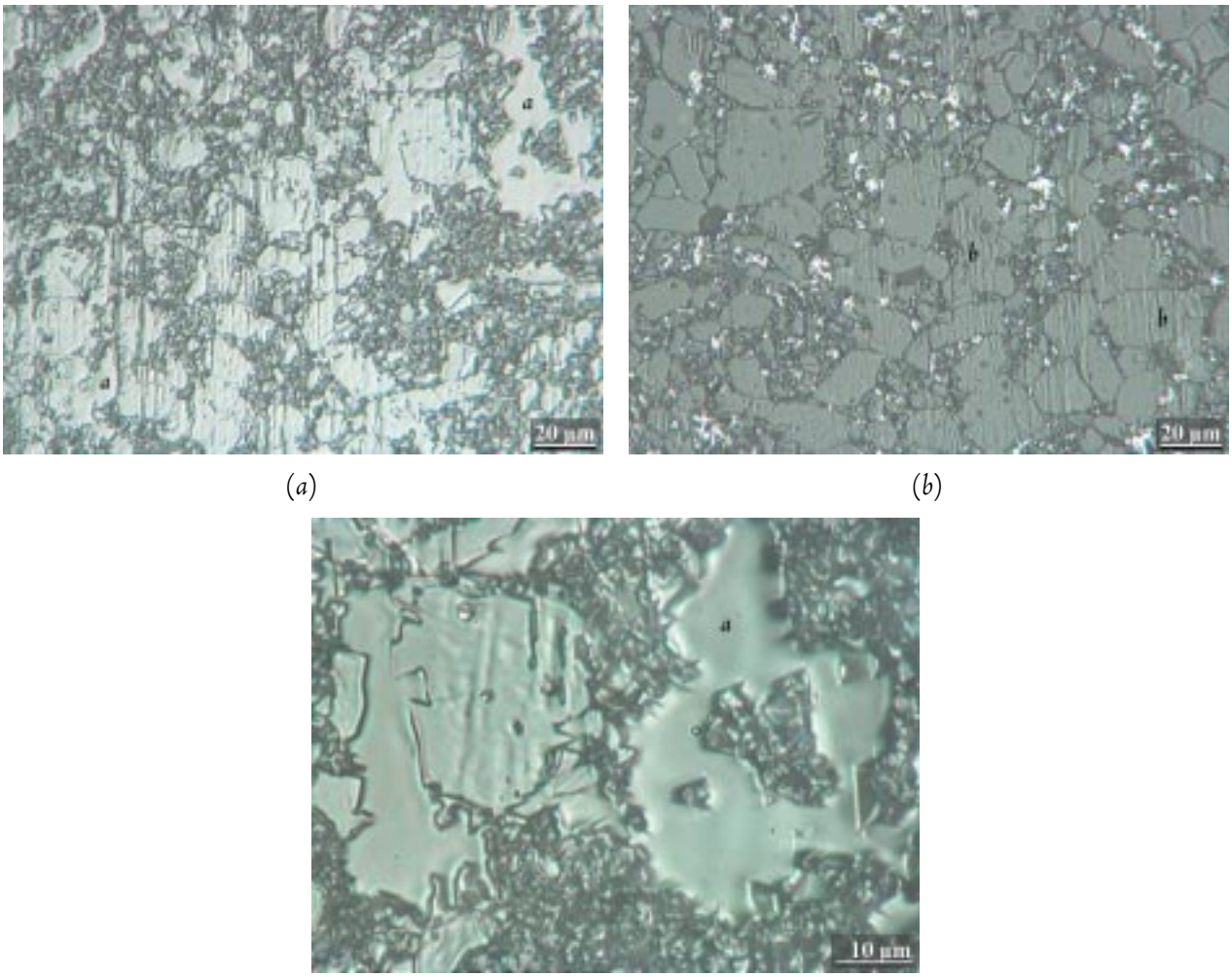

(*a*) (*b*)

(*c*)

FIGURE 2 Optical micrographs of matching regions of *a*) metal and *b*) ceramic sides of fracture surfaces of a diffusion-bonded sample that failed at 79 MPa. Regions of facetted contact growth in the upper right hand section of FIGURE 2*a* are shown at higher magnification in (*c*).

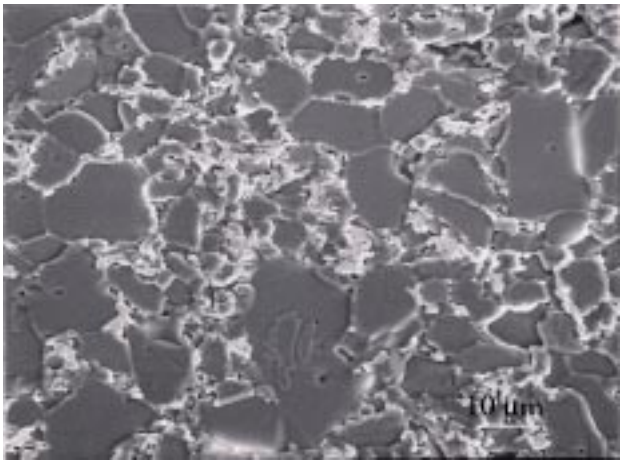

(*d*)

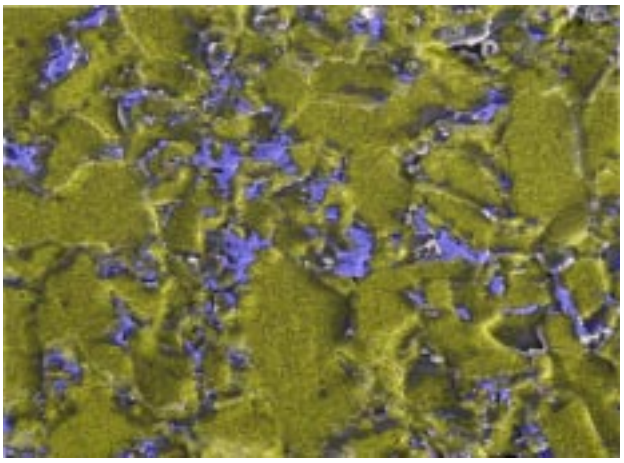

(*e*)

Figure 2 (*cont.*) Figures 2*d* and 2*e* show an SEM micrograph and an EDS map of the same location on the ceramic side of the fracture surface, respectively; the roughened regions on the fracture surface correspond to niobium (blue in the EDS map) adhering to the alumina (gold in the EDS map).

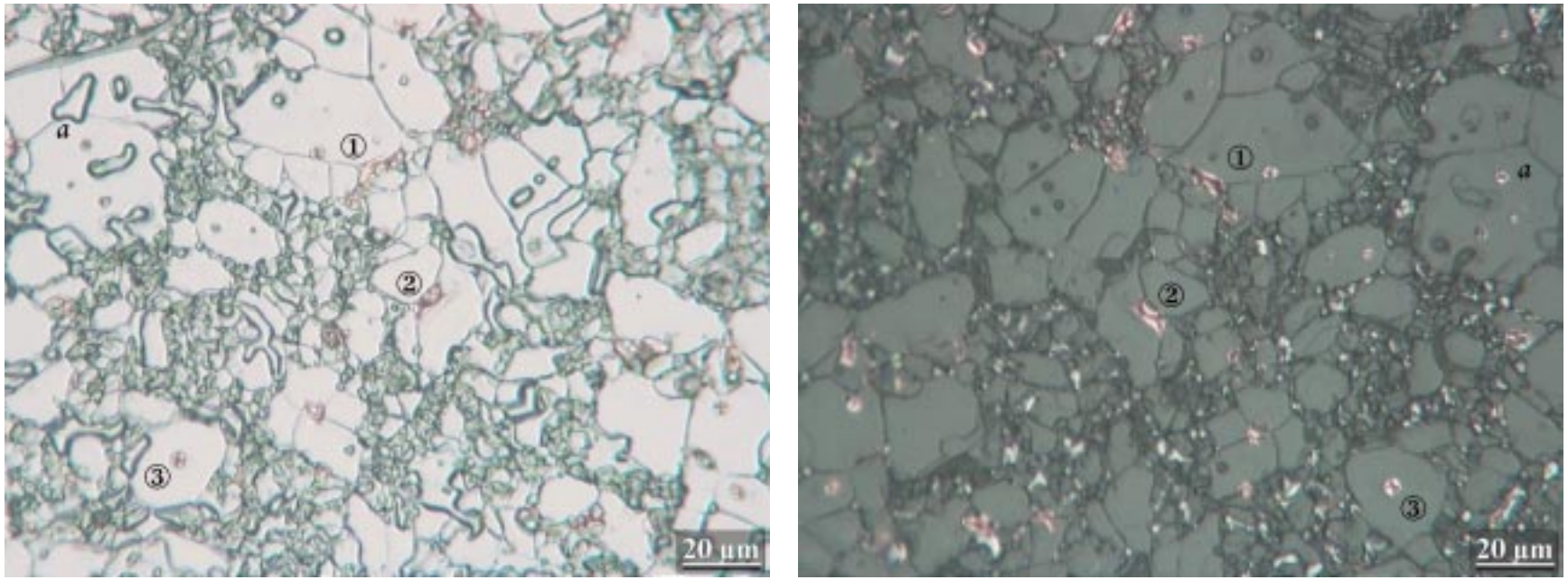

(*a*) (*b*)

FIGURE 3 Optical micrographs of matching regions of the *a*) metal and *b*) ceramic sides of fracture surfaces of a sample with 1.4-μm copper films assisting diffusion bonding. A more complete mapping of the ceramic grain structure onto the metal foil is evident. Matching regions of incomplete bonding are labeled ***a*** on both images; note the triple junction in the alumina is absent on the metal side due to an interfacial void that prevents contact. Most copper particles ruptured during fracture, and copper is thus present on both sides of the fracture surface; some pairs are labeled ①, ②, and ③.

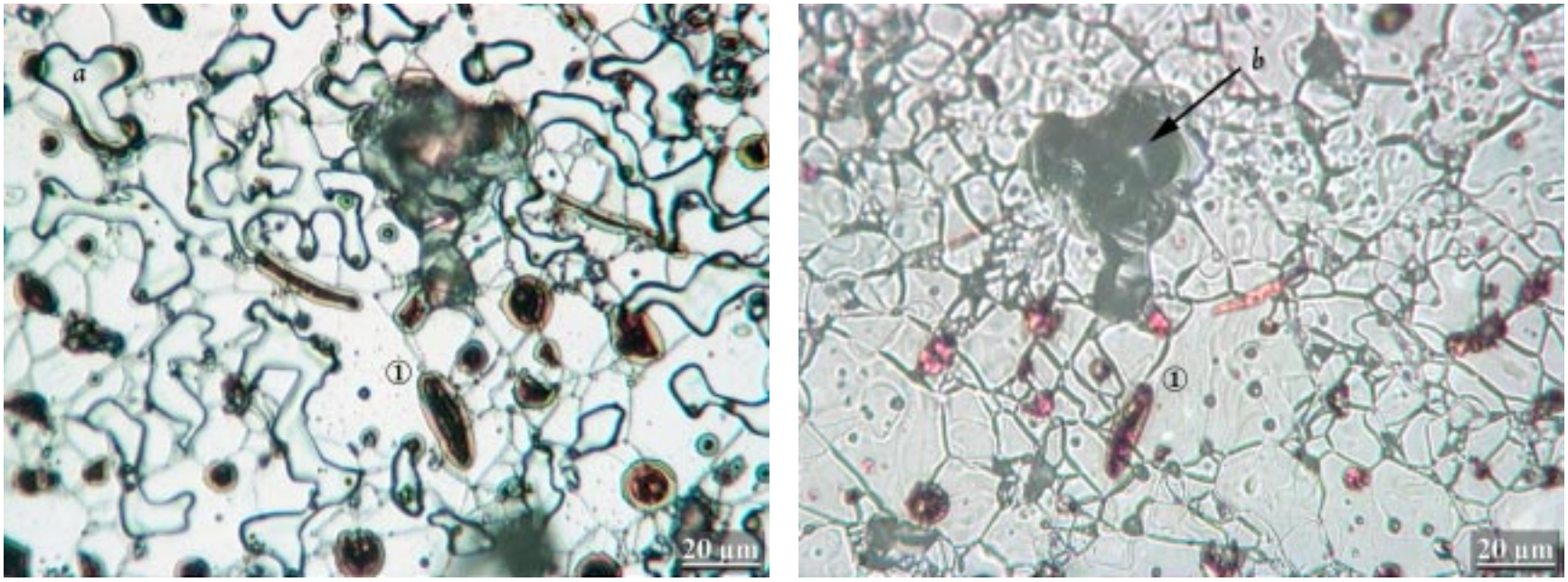

(*a*) (*b*)

FIGURE 4 Optical micrographs of matching regions of the *a*) metal and *b*) ceramic sides of fracture surfaces of a sample prepared with 3-μm thick copper films. Regions of incomplete bonding remain evident, one of which is labeled ***a*** in FIGURE 4*a*. The region marked ***b*** in FIGURE 4*b* represents an alumina grain that has been pulled out, and that has adhered to the metal side. Most copper particles ruptured during fracture and are present on both sides of the fracture surface; one pair is labeled ①.

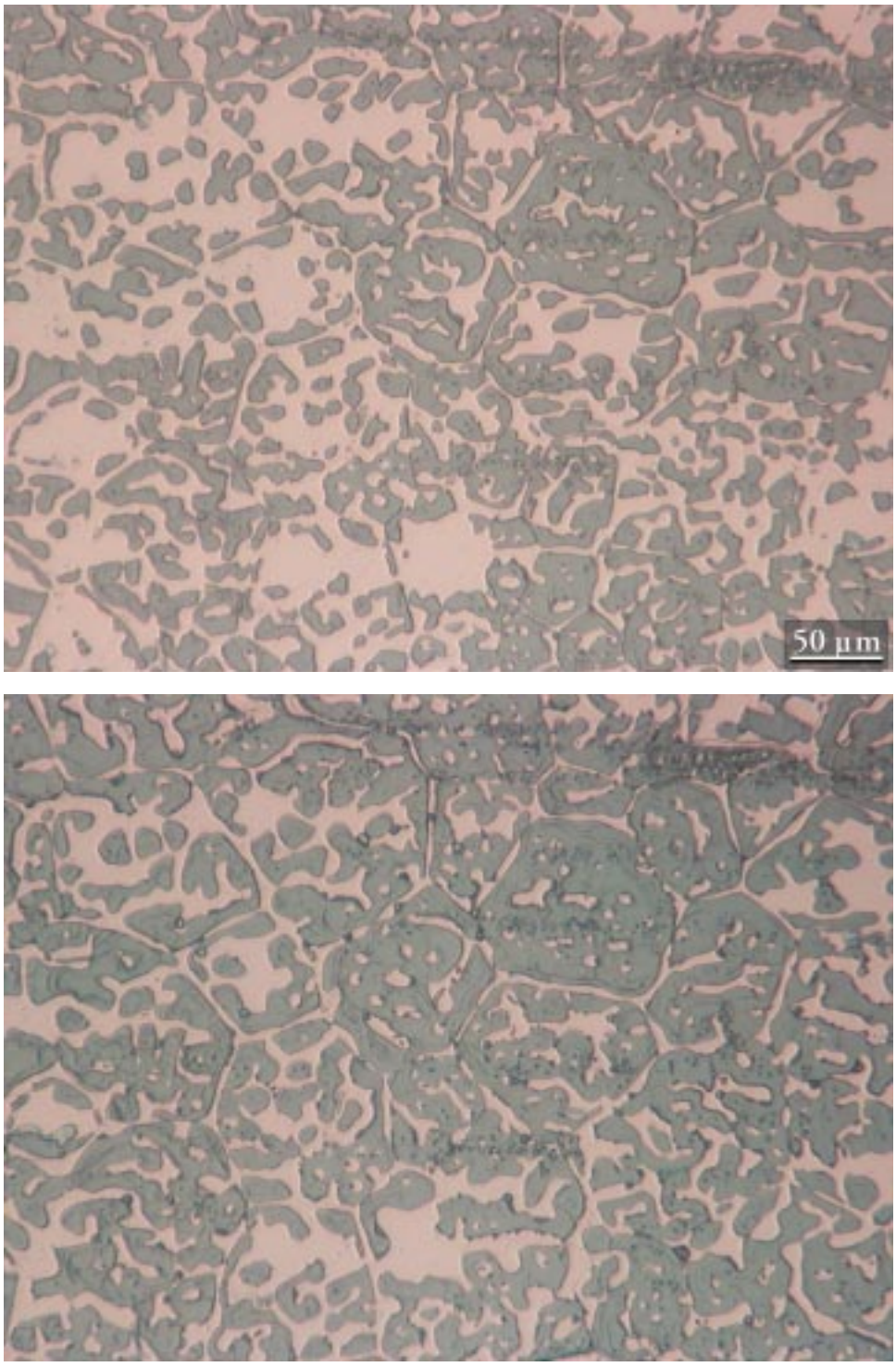

a)

b)

FIGURE 5 Illustration of interfacial microstructures in two sapphire/copper/niobium couples bonded at 1150°C. FIGURES 5*a* and 5*b* show the interfacial microstructure after 15 h at 1150°C, and after an additional 14 h of annealing at 1150°C, respectively. In this region, grain boundary groove ridges play a major role in initiating dewetting.

c)

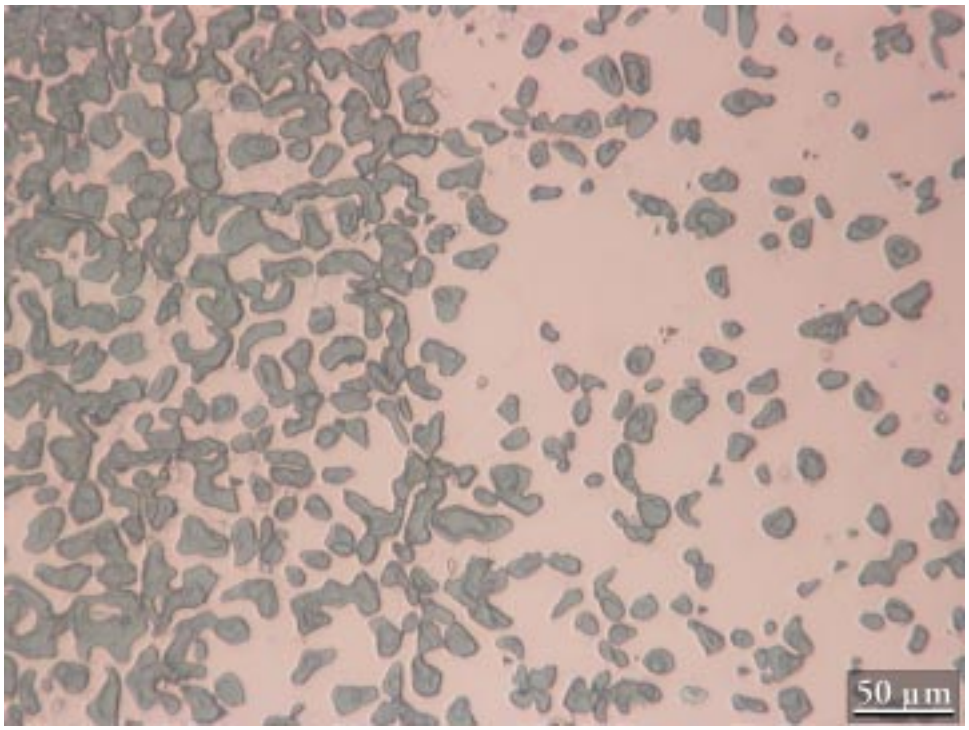

d)

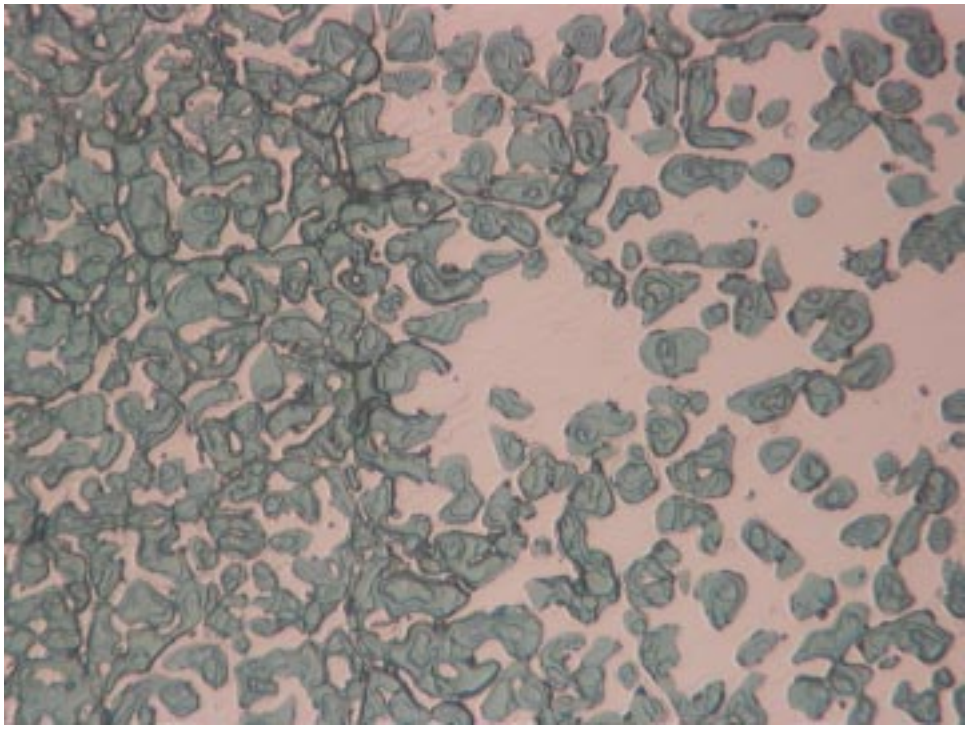

FIGURE 5 (*cont.*) In FIGURES 5*c* and 5*d*, also showing interfacial microstructures immediately after 15 h and 29 h at 1150°C, asperities appear to play a more prominent role in initiating dewetting.